Electronic Supplementary Information: Spin-forbidden heavy-atom tunneling in the ring-closure of triplet cyclopentane-1,3-diyl

Luís P. Viegas,* Cláudio M. Nunes and Rui Fausto

University of Coimbra, CQC, Department of Chemistry, 3004-535 Coimbra, Portugal

E-mail: lpviegas@ci.uc.pt

1 Nonparallelity Errors

In many situations the reasoning behind employing a model chemistry consisting of calculations of the type $\text{method}_2/\text{basis}_2//\text{method}_1/\text{basis}_1$ lies on the assumption that nonparallelity errors present in energy differences between stationary points are small or cancel out in a large extent. While this assumption should hold in many energy differences involving only minimum structures, it should not be expected to hold, for example, in the calculation of every single barrier height, since the topology of PESs in the saddle-point region is extremely sensitive to the method used for the optimization. Huge nonparallelity errors may be encountered when using popular model chemistries[1] to calculate barrier heights.

A close inspection of Table S1 reveals two important details. The first is that the MECP single-point energies at the MC-QDPT level are different (0.17 kcal mol^{-1} difference between the singlet and the triplet) instead of reproducing the degeneracy obtained at the CASSCF level. The second is that, at the MC-QDPT level, the energy difference between ^{1}**7a** and ^{1}**6a** is reduced from 1.6 kcal mol^{-1} at the CASSCF level to 0.57 kcal mol^{-1} at the MC-QDPT level. This raises some concerns about possible nonparallelity errors which gain particular importance in light of the low energy of the MECP compared to the ^{3}**2a** minimum. To shed some light on this problem we calculated MC-QDPT single-point energies on some selected geometries along the singlet IRC path obtained at the CASSCF level. The results are shown in Figure S1. In the minimum region the two curves are almost parallel, raising few concerns with respect to the location of the true minimum of the MC-QDPT curve. However, in the saddle-point region, the difference between the two curves is obvious. At the MC-QDPT level, a single-point energy calculation in the ^{1}**7a** CASSCF saddle-point geometry ($s = 0$ in this figure) seems to correspond to a region in the PES past the true MC-QDPT saddle-point (which is probably located close to $s = 1$) and on the path to the products. Since at the CASSCF level the MECP is very similar in geometry and energy to the ^{1}**7a** saddle-point, one might argue that the difference in the MC-QDPT energies for the MECP is also a consequence of such nonparallelity errors. Consequently, and because the MECP is low in energy, we employed the safer approach of not including dynamical correlation in the MECP height entering the rate constants

calculations, since it would carry a dangerously uncertain nonparallelity error. Instead, we considered the CASSCF(10,10)/cc-pVTZ energies alone, thus making sure that the energy difference is topologically sound.

2 Rate Constant Calculations

This section will consist of a more detailed version of Section 2.4 of the manuscript which closely follows the formalism presented in the tutorial review by Lykhin et al.[2] According to non-adiabatic transition state theory (NA-TST),[3–9] the ISC canonical temperature-dependent rate constant can be written as[2]

$$k_{\mathrm{ISC}}(T) = \frac{Q_{\mathrm{MECP}}(T)}{hQ_{\mathrm{R}}(T)} \int_0^\infty P_{\mathrm{trans}}(\varepsilon_\perp) \exp(-\beta\varepsilon_\perp) \mathrm{d}\varepsilon_\perp \tag{1}$$

where Q_{MECP} and Q_{R} are the partition functions at the MECP and reactant, respectively, $\beta = 1/k_{\mathrm{B}}T$, P_{trans} is the probability of transition between two states at the MECP and $\varepsilon_\perp$ is the component of the internal energy accumulated in the reaction coordinate.

The probability of transition between two adiabatic (mixed-spin) PESs can be calculated with the Landau-Zener (LZ) formula[10–12]

$$p^{\mathrm{LZ}}(\varepsilon_\perp) = \exp\left(-\frac{2\pi H_{\mathrm{SO}}^2}{\hbar|\Delta\mathbf{G}|}\sqrt{\frac{\mu_\perp}{2(\varepsilon_\perp - E_{\mathrm{MECP}})}}\right) \tag{2}$$

where $\mu_\perp$ is the reduced mass of the mode orthogonal to the crossing seam surface, E_{MECP} is the energy (total electronic energy plus ZPE) of the MECP relative to the minimum of the (triplet) spin-diabatic state where the reaction initiates (reactant R, in this case $^3\mathbf{2}$) defined as

$$E_{\mathrm{MECP}} = E_{\mathrm{MECP}}^{\mathrm{total}} + E_{\mathrm{MECP}}^{\mathrm{ZPE}} - (E_{\mathrm{R}}^{\mathrm{total}} + E_{\mathrm{R}}^{\mathrm{ZPE}}), \tag{3}$$

H_{SO} is the SOC constant and $|\Delta\mathbf{G}|$ is norm of the difference of the gradients on the two surfaces at the MECP, $|\Delta\mathbf{G}| = |\mathbf{G_1} - \mathbf{G_2}|$, which is orthogonal to the seam at the MECP. Here we are interested in calculating the probability of transition between the triplet and the singlet, i.e., the two spin-diabatic PESs, which is then $1 - p^{\mathrm{LZ}}$ and is often written considering the double passage version of the spin-diabatic LZ formula,

introduced to describe unimolecular decomposition[3]

$$\begin{aligned} P^{\mathrm{LZ}}_{\mathrm{trans}}(\varepsilon_{\perp}) &= (1-p^{\mathrm{LZ}}) + p^{\mathrm{LZ}}(1-p^{\mathrm{LZ}}) \\ &= 1-(p^{\mathrm{LZ}})^2 \end{aligned} \tag{4}$$

where $(1-p^{\mathrm{LZ}})$ is the probability of hopping on the first passage, and $p^{\mathrm{LZ}}(1-p^{\mathrm{LZ}})$ the probability for not hopping on first crossing the seam and then hopping upon crossing it again in the reverse direction.[2,13] Note that in Eq. (2), $p^{\mathrm{LZ}}(\varepsilon_{\perp})$ is defined only when the $\varepsilon_{\perp}$ internal energy is above the MECP ($\varepsilon_{\perp} > E_{\mathrm{MECP}}$), failing at energies in the vicinity of E_{MECP} and neglecting transitions between PESs caused by quantum tunneling for energies below E_{MECP}. This means that the LZ formula does not consider the fact that the system does not need to reach the crossing region to hop from one spin-diabatic PES to the other, but may instead tunnel across. Naturally, such energy regimes can be of extreme importance when performing studies at cryogenic temperatures, since a thermal over-the-barrier process will most likely be ruled out in the vast majority of cases. The interference between multiple reaction trajectories, which should lead to the oscillatory behavior of $P^{\mathrm{LZ}}_{\mathrm{trans}}$ for reaction energies larger than E_{MECP}, is also missing.[3] The details described above can be visualized in Figure 3 of Ref. 2.

The quantum effects mentioned above can be accounted for in the more robust double passage weak coupling (WC) probability expression[3,14,15]

$$P^{\mathrm{WC}}_{\mathrm{trans}}(\varepsilon_{\perp}) = 4\pi^2 H^2_{\mathrm{SO}} \left(\frac{2\mu_{\perp}}{\hbar^2 \bar{G} |\Delta \mathbf{G}|} \right)^{2/3} \mathrm{Ai}^2(\xi) \tag{5}$$

where $\bar{G} = \sqrt{|\mathbf{G_1}| \times |\mathbf{G_2}|}$ is the geometric mean of the norms of the gradients of the two PESs and $\mathrm{Ai}(\xi)$ is the Airy function (arising from an approximation to the overlap of vibrational wavefunctions[6,14]) with argument ξ which takes the form

$$\xi = -(\varepsilon_{\perp} - E_{\mathrm{MECP}}) \left(\frac{2\mu_{\perp} |\Delta \mathbf{G}|^2}{\hbar^2 \bar{G}^4} \right)^{1/3} \tag{6}$$

The WC expression for P_{trans} will then yield non-zero values for energies below E_{MECP}, although it decreases rapidly in this regime, allowing for tunneling from one PES to the other below the crossing point. Note that besides the vibrational analysis of the MECP, the GLOWfreq[16] code also yields $\mu_{\perp}$, $|\Delta \mathbf{G}|$ and $\bar{G}$, which are necessary

quantities to the LZ and WC probability expressions. This information is presented in Table S3.

Being a probability, the WC formula in Eq. (5) needs to obey to the relation $P_{\text{trans}}^{\text{WC}} \leq 1$ in order to be physically correct. Using Eq. (5) and taking its square root leads to the following condition[2]

$$2^{4/3}\pi \text{Max}[\text{Ai}(\xi)] H_{\text{SO}} \left(\frac{\mu_{\perp}}{\hbar^2 \bar{G} |\Delta \mathbf{G}|} \right)^{1/3} \leq 1 \tag{7}$$

where $\text{Max}[\text{Ai}(\xi)] \approx 0.5357$ is the maximum value of the Airy function which occurs[17] for $\xi = -1.0188$. Eq. (7) sets the limits of the WC formula, which may be problematic for systems with strong coupling, large reduced mass associated with the reaction coordinate, or small gradients. For this reason, the condition expressed by Eq. (7) should be checked before the actual WC rate constant calculation.

In summary, two rate constants were calculated in this work. The LZ rate constant

$$k_{\text{ISC}}^{\text{LZ}}(T) = \frac{Q_{\text{MECP}}(T)}{hQ_{\text{R}}(T)} \int_{E_{\text{MECP}}}^{\infty} P_{\text{trans}}^{\text{LZ}}(\varepsilon_{\perp}) \exp(-\beta \varepsilon_{\perp}) \text{d}\varepsilon_{\perp} \tag{8}$$

which is important for comparison reasons as it operates only in the classically allowed region for energies above the MECP, therefore excluding possible tunneling effects. The other is the more robust WC rate constant

$$k_{\text{ISC}}^{\text{WC}}(T) = \frac{Q_{\text{MECP}}(T)}{hQ_{\text{R}}(T)} \int_{0}^{\infty} P_{\text{trans}}^{\text{WC}}(\varepsilon_{\perp}) \exp(-\beta \varepsilon_{\perp}) \text{d}\varepsilon_{\perp} \tag{9}$$

which gathers contributions from both the classically allowed, $E_{\text{MECP}} < \varepsilon_{\perp} < \infty$, and classically forbidden (tunneling) regions, $0 < \varepsilon_{\perp} < E_{\text{MECP}}$. It then becomes possible to write the integral of the previous equation as

$$\int_{0}^{E_{\text{MECP}}} P_{\text{trans}}^{\text{WC}}(\varepsilon_{\perp}) \exp(-\beta \varepsilon_{\perp}) \text{d}\varepsilon_{\perp} + \int_{E_{\text{MECP}}}^{\infty} P_{\text{trans}}^{\text{WC}}(\varepsilon_{\perp}) \exp(-\beta \varepsilon_{\perp}) \text{d}\varepsilon_{\perp} \tag{10}$$

and evaluate the contribution of each region to the rate constant value.

All theoretical rate constant values are shown in Table S4, which were used to generate the Arrhenius plots of Figure 3 of the manuscript. Interestingly, certain parallelisms can be drawn between the two curves shown in Figure 3 and the curves shown in typical Arrhenius plots[18–21] for spin-allowed reactions where heavy-atom tunneling plays an important role: the LZ rate constants can be associated with the canonical variational transition state theory (CVT)[22] rate constants while a similar

association can be made between the WC rate constants and the CVT rate constants including small-curvature tunneling.[22,23]

Along with the experimental rate constants reported in a recent work,[21] a theoretical rate constant was also calculated in the same paper for the reaction S-**DR** (**^{1}6**) to **CP** (**^{1}8**). The initial result, based on canonical variational theory with small-curvature tunneling, yielded a rate constant of 1.3×10^2 s^{-1}. However, the S-**DR** minimum cannot possibly be populated at cryogenic temperatures. With this in mind, the authors used a trick to simulate the same reaction as if it was starting from their calculated triplet state, T-**DR** (**^{3}2**), proceeding to report a rate constant of 5.2 s^{-1} including tunneling corrections. This trick consisted of artificially increasing the barrier from S-**DR** to **CP** by 0.64 kcal mol^{-1}, which is the energy difference between S-**DR** and T-**DR** at the B3LYP/6-31G(d) level. However, and as stated by the authors, such an approach does not explicitly take into account the spin-forbidden nature of the reaction, which complicates the interpretations associated to this result. The good agreement between their theoretical rate constant and the rate constants in argon matrices stems from the fact that at the DFT level the **^{1}7** saddle-points are considerably higher in energy with respect to the **^{1}6** minima (3.03 kcal mol^{-1} at the B3LYP/6-31G(d) level[21] and 2.95 kcal mol^{-1} at the M06-2X/pcseg-2 level obtained in exploratory calculations performed this work) when compared to the same energy difference at the CASSCF(10,10)/cc-pV*T*Z level, which is 1.32 kcal mol^{-1}. Consequently, this larger value for the barrier height which is then artificially extended by 0.64 kcal mol^{-1} accidentally contributes to the lowering of their rate constant to a value close to the observed in argon matrices.

However, it should be stressed that the height of the MECP, which is the true bottleneck of this reaction, is actually even lower at the M06-2X/pcseg-2 level (1.05 kcal mol^{-1}) than at the CASSCF(10,10)/cc-pV*T*Z level (1.68 kcal mol^{-1}), most likely leading to even larger values for the rate constants at the DFT level, not lower. In our opinion, the correct way to calculate these rate constants is to employ a model that accounts for tunneling and also the change in spin multiplicity, such as the WC formulation of NA-TST.

It should be noted, as pointed out by Harvey,[24] that because NA-TST is a statistical rate theory strongly related to transition state theory, besides its own approximations

“it suffers from many of the same assumptions and approximations as the latter, and cannot be expected to yield exact results." It is then reasonable to expect that rate constants calculated with NA-TST are many times within one order of magnitude of the exact value. Adding to the fact that we are calculating gas-phase rate constants and comparing them to a matrix environment, it should also be noted that all parameters in the NA-TST equation were determined without including dynamical correlation energy. Parameters such as the MECP height, SOC, gradients and Hessians at the MECP will vary with the inclusion of dynamical correlation, shifting the values of the rate constants (sometimes to a considerable extent) but keeping the same qualitative trends shown in Figure 3 of the manuscript.

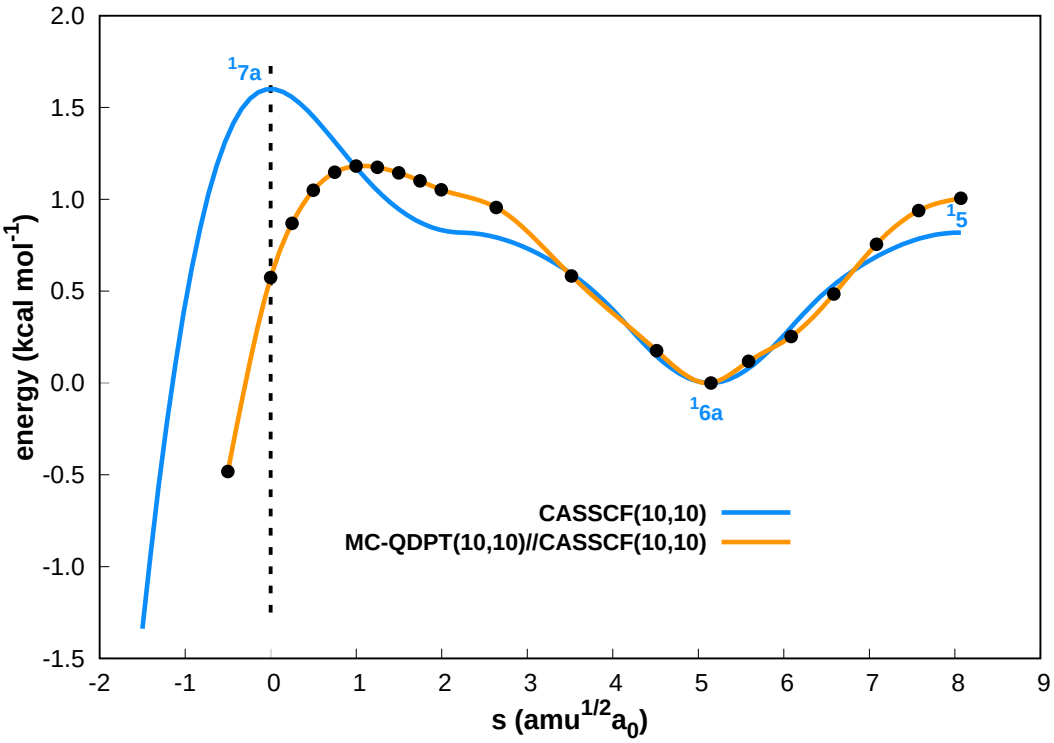

Figure S1. Schematic diagram illustrating the nonparallelity between part of the CASSCF(10,10)/cc-pV*T*Z singlet IRC path and the potential curve resulting from interpolating 20 points along the optimized IRC path at the MC-QDPT(10,10)/cc-pV*T*Z//CASSCF(10,10)/cc-pV*T*Z level.

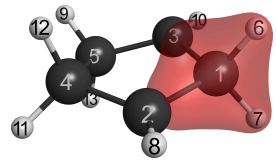

MO15(1.98)

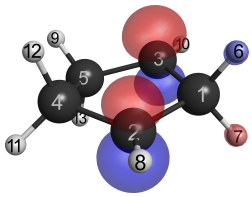

MO20(1.00)

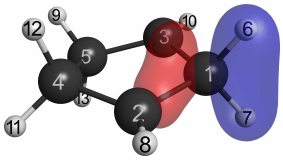

MO16(1.98)

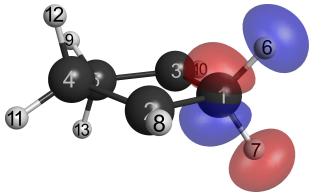

MO21(0.02)

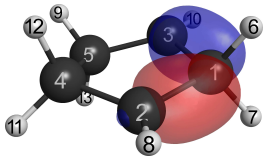

MO17(1.98)

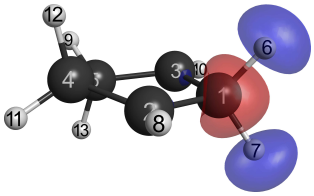

MO22(0.02)

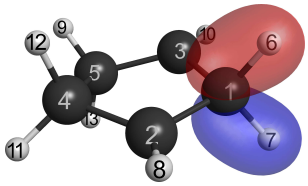

MO18(1.98)

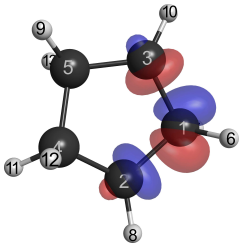

MO23(0.02)

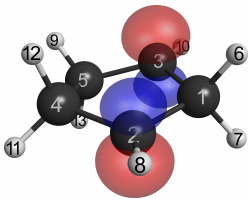

MO19(1.00)

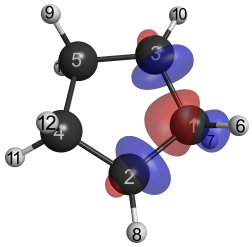

MO24(0.02)

Figure S2. CASSCF natural orbitals and their occupation numbers for the active space of the ^{3}**2a** minimum. The structures showing the σ^{*} molecular orbitals (MOs) are slightly reoriented so that the nodes are clearly visible.

Table S1. Total energies ($E^{\text{MC-QDPT}}$ obtained with the cc-pVTZ basis set at the CASSCF(10,10)/cc-pVTZ stationary points), ZPEs, relative energies ($\Delta E^{\text{MC-QDPT}}$) with respect to the **^{3}2a** minimum and imaginary frequencies ($\nu^{\ddagger}$) of saddle-points for all structures in panel a) of Figures 1 and 2 of the manuscript.

Stationary point	$E^{\text{MC-QDPT}}$/E$_h$	ZPE/E$_h$	$\Delta E^{\text{MC-QDPT}}$/kcal mol^{-1}	$\nu^{\ddagger}$/cm^{-1}
^{3}1	-194.7920038044	0.115227	0.27	122.4
^{3}2a	-194.7931827239	0.115977	0.00	-
^{3}3a	-194.7349015581	0.114065	35.37	719.3
^{3}4a	-194.7493391719	0.114524	26.60	-
^{1}5	-194.7894138373	0.115596	2.13	111.0
^{1}6a	-194.7910165982	0.116239	1.52	-
^{1}7a	-194.7901019707	0.115787	1.81	238.8
^{1}8a	-194.8537191902	0.120639	-35.06	-
^{1}MECP$_a$	-194.7893165373	0.114431	1.46	-
^{3}MECP$_a$	-194.7890439610	0.114431	1.63	-

Table S2. Leading determinants (with reference coefficients greater than 0.05) of the CASSCF wavefunctions of some relevant structures.

Structure	Determinant	Coefficient
^{3}**2a**	2222aa0000	0.971828
	2220aa0200	-0.053785
	2022aa2000	-0.057203
^{1}**6a**	2222ab0000	0.968749
	2220ab0200	-0.066651
	2a222b0000	0.071060
	2a22b20000	-0.066647
	2022ab2000	-0.055616
^{1}**MECP$_a$**	2222200000	-0.592289
	2222ab0000	-0.648882
	2222020000	0.407146
	2a22b20000	-0.088931
^{3}**MECP$_a$**	2222aa0000	-0.971729
	2220aa2000	0.056536
	2022aa0200	0.058074

Table S3. Data used for the Landau-Zener (LZ) and weak coupling (WC) probability expressions of Eqs. (2) and (5) obtained at the CASSCF/cc-pVTZ level. The last entry shows the maximum probability associated with Eq. (5) and determines its validity according to Eq. (7).

	CASSCF(10,10)/cc-pVTZ
E_{MECP}/kcal mol^{-1}	1.68
H_{SO}/cm^{-1}	0.34
$\mu_{\perp}$/amu	11.81
$\lvert\Delta\mathbf{G}\rvert$/hartree bohr^{-1}	2.26×10^{-2}
$\bar{G}$/hartree bohr^{-1}	1.33×10^{-2}
Max. WC probability	2.73×10^{-3}

Table S4. Theoretically determined gas-phase rate constants for the ring-closure of triplet cyclopentane-1,3-diyl to singlet bicyclo[2.1.0]pentane at different temperatures with the LZ and the WC formulations of NA-TST.

Temperature/K	$k_{\mathrm{ISC}}^{\mathrm{LZ}}(T)/\mathrm{s}^{-1}$	$k_{\mathrm{ISC}}^{\mathrm{WC}}(T)/\mathrm{s}^{-1}$
5	8.54×10^{-68}	3.56×10^{2}
6	1.60×10^{-55}	4.31×10^{2}
7	9.46×10^{-47}	5.08×10^{2}
8	3.62×10^{-40}	5.86×10^{2}
9	4.80×10^{-35}	6.66×10^{2}
10	6.05×10^{-31}	7.47×10^{2}
13	2.03×10^{-22}	1.00×10^{3}
17	1.02×10^{-15}	1.37×10^{3}
20	1.93×10^{-12}	1.67×10^{3}
25	1.02×10^{-8}	2.23×10^{3}
30	3.17×10^{-6}	2.88×10^{3}
50	3.51×10^{-1}	6.83×10^{3}
100	2.75×10^{3}	3.84×10^{4}
150	5.99×10^{4}	1.55×10^{5}
200	2.86×10^{5}	4.39×10^{5}
250	7.36×10^{5}	9.21×10^{5}
300	1.38×10^{6}	1.58×10^{6}
350	2.17×10^{6}	2.36×10^{6}
400	3.03×10^{6}	3.20×10^{6}
450	3.92×10^{6}	4.08×10^{6}
500	4.81×10^{6}	4.94×10^{6}

References

[1] L. P. Viegas and A. J. C. Varandas, *J. Comput. Chem.*, 2014, **35**, 507–517.

[2] A. O. Lykhin, D. S. Kaliakin, G. E. dePolo, A. A. Kuzubov and S. A. Varganov, *Int. J. Quantum Chem.*, 2016, **116**, 750–761.

[3] J. B. Delos, *J. Chem. Phys.*, 1973, **59**, 2365–2369.

[4] J. C. Tully, *J. Chem. Phys.*, 1974, **61**, 61–68.

[5] G. E. Zahr, R. K. Preston and W. H. Miller, *J. Chem. Phys.*, 1975, **62**, 1127–135.

[6] E. J. Heller and R. C. Brown, *J. Chem. Phys.*, 1983, **79**, 3336–3351.

[7] J. C. Lorquet and B. Leyh-Nihant, *J. Phys. Chem.*, 1988, **92**, 4778–4783.

[8] J. N. Harvey and M. Aschi, *Phys. Chem. Chem. Phys.*, 1999, **1**, 5555–5563.

[9] Q. Cui, K. Morokuma, J. M. Bowman and S. J. Klippenstein, *J. Chem. Phys.*, 1999, **110**, 9469–9482.

[10] L. D. Landau, *Phys. Z. Sowjetunion*, 1932, **2**, 46–51.

[11] C. Zener, *Proc. R. Soc. Lond. A*, 1932, **137**, 696–702.

[12] J. C. Tuly, *J. Chem. Phys.*, 2012, **137**, 22A301.

[13] J. N. Harvey and M. Aschi, *Faraday Discuss.*, 2003, **124**, 129–143.

[14] L. D. Landau and E. M. Lifshitz, *Quantum Mechanics. Non-relativistic Theory*, Pergamon Press Ltd., Oxford, England, Second (revised) edn, 1965.

[15] P. V. Coveney, M. S. Child and A. Bárány, *J. Phys. B: At. Mol. Phys.*, 1985, **18**, 4557–4580.

[16] K. L. Gannon, M. A. Blitz, C.-H. Liang, M. J. Pilling, P. W. Seakins, D. R. Glowacki and J. N. Harvey, *Faraday Discuss.*, 2010, **147**, 173–188.

[17] K. W. Ford and J. A. Wheeler, *Ann. Phys.*, 1959, **7**, 259–286.

[18] P. S. Zuev, R. S. Sheridan, T. V. Albu, D. G. Truhlar, D. A. Hrovat and W. T. Borden, *Science*, 2003, **299**, 867–870.

[19] A. Datta, D. A. Hrovat and W. T. Borden, *J. Am. Chem. Soc.*, 2008, **130**, 6684–6685.

[20] C. S. Michel, P. P. Lampkin, J. Z. Shezaf, J. F. Moll, C. Castro and W. L. Karney, *J. Am. Chem. Soc.*, 2019, **141**, 5286–5293.

[21] S. K. Sarkar, E. Solel, S. Kozuch and M. Abe, *J. Org. Chem.*, 2020, **85**, 8881–8892.

[22] J. L. Bao and D. G. Truhlar, *Chem. Soc. Rev.*, 2017, **46**, 7548–7596.

[23] Y.-P. Liu, G. C. Lynch, T. N. Truong, D.-H. Lu, D. G. Truhlar and B. C. Garret, *J. Am. Chem. Soc.*, 1993, **115**, 2408–2415.

[24] J. N. Harvey, *WIREs Comput. Mol. Sci.*, 2014, **4**, 1–14.